

Building Blocks in Hierarchical Clustering Scenarios and their Connection with Damped Ly α Systems

Sofía A. Cora,^{1,2,5} Patricia B. Tissera,^{2,3} Diego G. Lambas,^{2,4,6} and Mirta B. Mosconi,⁴

¹ *Facultad de Ciencias Astronómicas y Geofísicas de la Universidad Nacional de La Plata, Argentina.*

² *Consejo Nacional de Investigaciones Científicas y Técnicas, Argentina.*

³ *Instituto de Astronomía. y Física del Espacio, Argentina.*

⁴ *Observatorio Astronómico de la Universidad Nacional de Córdoba, Argentina.*

⁵ *Postdoctoral Fellow of Fundación Antorchas at Max-Planck Institute for Astrophysics, Germany.*

⁶ *John Simon Guggenheim Fellow.*

19 June 2018

ABSTRACT

We carried out a comprehensive analysis of the chemical properties of the interstellar medium (ISM) and the stellar population (SP) of current normal galaxies and their progenitors in a hierarchical clustering scenario. We compared the results with observations of Damped Lyman- α systems (DLAs) under the hypothesis that, at least, part of the observed DLAs could originate in the building blocks of today normal galaxies. We used a hydrodynamical cosmological code which includes star formation and chemical enrichment. Galaxy-like objects are identified at $z = 0$ and then followed back in time. Random line-of-sights (LOSs) are drawn through these structures in order to mimic Damped Lyman α systems. We then analysed the chemical properties of the ISM and SP along the LOSs. We found that the progenitors of current galaxies in the field with mean $L < 0.5L^*$ and virial circular velocity of 100 – 250 km/sec could be the associated DLA galaxies. For these systems we detected a trend for $\langle L/L^* \rangle$ to increase with redshift. We found moderate metallicity evolution for the [Zn/H], [Fe/H] and [Si/H]. However, when we applied the observational filter suggested by Boissé et al. (1998) in order to restrict the sample to the observed limits in densities and metallicities, we found mild evolution consistent with observational results that include dust corrections. The [Si/Fe] and [S/Fe] show weak α -enhancement in agreement with observations corrected by dust depletion. We found the α /Fe in the ISM and SP to have more homogeneous abundances than the [Fe/H] and [Zn/H] ones. In our models, the global metallicity evolution is driven by the high metallicity and high column density simulated DLAs which have low impact parameters ($b < 5$ kpc) and SPs with more than $10^8 M_\odot$. Our results suggest that geometrical effects could be the mechanism responsible for the non-detectability of high metallicity and high column density DLAs. We found sub-DLAs to map preferentially the outskirts of the simulated DLA galaxies. Hence, they can contribute to the study of the metallicity of the galactic structure as a function of redshift. An analysis of the metallicity content of the ISMs and SPs of the galaxy-like objects as a function of redshift show the formation of a central stellar mass concentration with nearly solar metallicity at all redshift while stars in the outer parts of these objects have lower metallicities. The gas content gets enriched progressively with redshift and at all radii. The abundance properties of the galaxy-like objects and the simulated DLAs are the results of the contribution of supernovae type Ia and type II and gas infall from the dark matter haloes with a timing settled by their particular history of evolution in a hierarchical clustering scenario. Our results suggest that the mild evolution detected in the observations could arise from a conspiracy of all these processes.

Key words: cosmology: theory - galaxies: formation - galaxies: evolution - galaxies: abundances.

arXiv:astro-ph/0304303v2 25 Apr 2003

1 INTRODUCTION

Our understanding of the Universe has improved dramatically in the last decades due to the outstanding discoveries made by large orbiting and ground-based telescopes. In particular, Damped Ly α absorptions identified in the spectra of distant quasars provide clues on the chemical and kinematic properties of systems at different redshifts. However, the nature of the host of the absorbing neutral hydrogen (H I) clouds (hereafter DLA galaxies) remains unclear. At low redshift, identified DLAs are associated with galaxies of different morphologies with a preference for dwarf and low surface brightness ones (Le Brun et al. 1997; Rao & Turnshek 2000), while at higher z , there is no clear evidence of the morphological characteristics of the DLA galaxies.

Different models have been proposed to explain the kinematics of DLAs. In particular, Haehnelt et al. (1998), by using hydrodynamical simulations, have found that the features in the velocity width distributions of these systems could be reproduced by the substructure in Cold Dark Matter models (see also MacDonald & Miralda-Escudé 1999). Other mechanisms have been suggested as responsible for producing such velocity distributions. Among them, Nulsen, Barcons & Fabian (1998) claimed that massive out-flows from dwarf galaxies could account for the majority of DLA systems in their semi-analytical models for galaxy formation (see also Schaye 2001a).

From the point of view of chemical evolution, abundance ratios suggest that DLAs are young systems with a low metallicity content which seems not to evolve significantly from very high z to present days (e.g., Prochaska & Wolfe 2002). However, several biasing factors may be affecting these conclusions. Dust depletion and obscuration are a main source of uncertainties for the determination of some element abundances (e.g., Vladilo 1998). However, the estimations of the amount of depletion and obscuration by dust for each element is a complex task which have produced different results (Vladilo 2002; Prochaska & Wolfe 2002). Another important effect is that DLAs with high metallicity and high column density are missing from the data (e.g., Boissé et al. 1998; Hou et al. 2001). Traditionally, the lack of these systems has been interpreted as a bias produced by dust obscuration. However, first analysis of DLAs identified from a radio selected QSO survey by Ellison et al. (2001) could suggest that such sort of DLAs might not be present at all in nature since the selection of this sample should not be dust biased. However, a larger database is needed before reaching a solid conclusion.

The chemical properties of the absorbers might be affected by different processes such as star formation, energy feedback, etc., and by different mixing mechanisms like those produced by tidal forces and mergers. These processes depend on the history of evolution of each galaxy which may be also affected by its environment (see Ellison & López 2001). Hence, it is not simple to envisage a model (e.g., Mathlin et al. 2001) to explain DLA properties and to relate them to the characteristics of the associated DLA galaxies, even more, if the internal structure of the systems and environmental effects ought to be taken into account.

DLAs observations provide clues on the chemical evolution of the observable neutral H mass in the Universe. Since the metallicity of the ISM is the result of the effects of dif-

ferent physical processes such as stellar evolution, mergers, interactions, collapses, etc., with some of them depending also on the cosmology, it is relevant for a galaxy formation model to be able to reproduce them. In this way, the individual and global chemical properties of the matter can be used as tests for galaxy formation and cosmological models. Hydrodynamical cosmological simulations are adequate tools to tackle these problems since the dynamical range that can be resolved allows the statistical description of internal properties of the galactic objects such as mass distributions and star formation histories, as well as mergers and interactions (see Somerville et al. 2001 for a semianalytical approach).

Tissera et al. (2001, Paper I) used a chemical model coupled to a hydrodynamical cosmological code to analyse the metallicity properties of the interstellar medium (ISM) of the galactic objects when mapped by random LOSs. These authors found that the chemical abundances obtained in such a way were comparable to those measured from DLAs observations. Their results support the hypothesis that at least part of the observed DLAs could originate in the building blocks of current normal galaxies, in agreement with those found by Haehnelt et al. (1998) from a kinematic analysis. In this paper we extend their work, making a more detailed analysis and comparison between the simulated and new observed DLAs. We also analyse comparatively the properties of the stellar populations intercepted by the LOSs and consequently associated to the DLAs, and those of the total stellar populations of their host galaxies.

2 NUMERICAL MODELS

The hydrodynamical chemical simulations analysed follow the joint evolution of dark matter and baryons within a cosmological context (Tissera et al. 1997), including star formation and chemical evolution. The hydrodynamical equations have been implemented in the AP3M gravitational code (Thomas & Couchman 1992) by using the Smooth Particle Hydrodynamics (SPH) technique. Baryons are initially assumed to be in the form of gas. Dense and gaseous regions in convergent flows are gradually transformed into stars at different star formation (SF) episodes, according to the Schmidt law. A star formation efficiency (ϵ) has to be assumed to regulate this process.

The chemical model used in this paper has been discussed in detail by Mosconi et al. (2001). Briefly, it is a self-consistent implementation that considers the chemical evolution of the SP and ISM taking into account the contributions of different SP generations. Type Ia (SNIa) and type II (SNII) supernovae are taken into account according to stellar evolution models and chemical enrichment yields. We adopted the yields given by Woosley & Weaver (1995) for SNII and by Thielemann, Nomoto & Hashimoto (1993) for SNIa. We assumed a fixed Salpeter Initial Mass Function with lower and upper mass cut-offs of $0.1 M_{\odot}$ and $120 M_{\odot}$, respectively. Chemical elements generated in a given particle are distributed within its neighboring area, weighting each contribution with a kernel function that depends on the relative distance between gaseous particles. The distribution of metals by using the SPH technique results in an effective mixing mechanism that allows the enrichment of re-

gions that are nearby to star-forming particles (see Lia et al. 2002 for a different implementation of the mixing process).

Although we stress the relevance of the energy injection into the interstellar medium due to supernovae explosions in the formation of the galaxies, we have not included this mechanism in this work. Several attempts to implement energy feedback in SPH codes can be found in the scientific literature (e.g., Katz 1992; Navarro & White 1994; Metzler & Evrard 1994; Navarro & Steinmetz 2000; Springel 2000), although they are still quite controversial.

The simulations studied in this paper followed the cosmological evolution of typical $5 h^{-1}$ Mpc ($h = 0.5$) cubic volumes represented by 64^3 equal mass particles ($M_p = 1.4 \times 10^8 h^{-1} M_\odot$). Initial conditions are consistent with a Standard Cold Dark Matter (SCDM) Universe ($\Omega = 1$, $\Omega_b = 0.10$, $H_0 = 100 h^{-1} \text{ km s}^{-1} \text{ Mpc}^{-1}$) with cluster abundance normalization, $\sigma_8 = 0.67$ and $\Lambda = 0$. We used a gravitational softening $\epsilon_g = 1.5$ kpc and a minimal smoothing length of $\epsilon_g/2$ (see Section 3.1 for a discussion on numerical effects).

In Paper I, we analysed a set of three simulations (S.2, S.6 and S.7), each one representing different realizations of the power spectrum run by Mosconi et al. (2001). As shown by these authors, at $z = 0$ these simulations reproduced galactic systems with mean metal abundances in agreement with observations. However, when the abundance patterns of the stellar populations in the individual galactic systems were analysed in detail, we found that none of them resembled fairly well that of the Milky-Way, although averaged abundances are within observed values. Therefore, we run a new simulation (S.8) with different SN parameters in order to be able to have systems with chemical abundance patterns similar to those of the Galaxy (i.e., we have increased c and the ratio between SNII and SNIa rates). For SNIa, we have adopted a life-time for progenitor binary systems of 0.5 Gyr. However, note that we do not know how common the Milky-Way abundance patterns are among similar morphological type galaxies (Wolfe et al. 2000), so we consider that both set of simulated objects can provide useful information about the chemical evolution of the structure in hierarchical clustering models. In this paper we will focus the analysis on simulation S.8.

3 SIMULATED DLA GALAXIES AND DLA SYSTEMS

Following the hypothesis that the progenitors of today normal galaxies in hierarchical scenarios could be the host galaxies of the observed DLAs, we carried out a comparative analysis of the mean chemical properties of the simulated DLA galaxies and DLA systems. The former are given by the ISM and SP residing in dark matter structures that are detected by an overdensity criterium. On the other hand, random LOSs are drawn through these structures following the observational procedure used to detect them. Simulated DLAs correspond to those LOSs that map regions where the neutral hydrogen column density $N(\text{H}_I)$ is greater than 10^{20} atoms/cm².

3.1 Galaxy-like Objects

We identified galactic objects at different stages of evolution of the simulated volumes. Firstly, a friend-of-friend method is used to isolate the higher density peaks in the mass distribution, and then, a density-contrast algorithm is applied to find over-densities with $\delta\rho/\rho \approx 200$. The selected galactic objects are the building blocks of today normal galaxies which grew by accretion and/or mergers. The rate of mergers as well as the distribution of merger parameters are determined by the cosmological model adopted. The main baryonic clump within a virialized structure will be, hereafter, referred to as the galaxy-like object (GLO), and it constitutes what we also call simulated DLA galaxy. GLOs have been truncated at two optical radius, $2R_{\text{opt}}$, where R_{opt} has been defined as the radius which encloses 83% of the baryonic mass.

For the purpose of diminishing numerical resolution problems, we analyse galactic objects with more than 200 baryonic particles within their virial radius and in the redshift range $0.25 < z < 2.35$. The final sample is made of 166 GLOs that satisfy the above conditions and have virial velocities within $\approx 100\text{--}250 \text{ km s}^{-1}$. Owing to the fact that all particles have the same mass, the selected objects have well resolved dark matter haloes (more than 2000 particles) providing well-defined potential wells onto which, on its turn, baryons can settle on (Steinmetz & White 1997). Hence, although the baryonic mass resolution is low compared to other simulations (e.g., Cen et al. 2003), the gaseous density profiles are well described. This is an important point since the star formation rate and, consequently, the metal production, is proportional to the gas density (e.g., Tissera 2000), and hence it depends on how well the profiles are described.

As a combined result of dynamical evolution, mergers and interactions, the SF rate history of each galactic object in hierarchical clustering scenarios can be described as a contribution of an ambient SF rate and a series of starbursts (e.g., Tissera 2000). In our models, the timing between starbursts are given naturally by the evolution of the objects in the hierarchical clustering scenario adopted. As discussed by Tissera (2000 and references therein), Tissera et al. (2001) and suggested by recent observations (e.g., Barton, Geller & Kenyon 2000; Le Fevre et al. 2000; Lambas et al. 2003) mergers and interactions play a crucial role in triggering SF and consequently, may leave important imprints in the chemical patterns of galaxies (Prantzos & Boissier 2000). Our model provides a consistent description of these processes as well as including the contributions of SNIa and SNII consistently with the SF histories of the objects.

In order to understand how metals are distributed within the GLOs, we have considered concentric shells centred at the GLO mass centre. The shells have an outer fixed radius of $2R_{\text{opt}}$ and an inner radius r , which varies from $r = 0$ to $r = 10$ kpc. For each shell, we define the H_I mass-weighted mean abundance ratio of elements K and J, $[\text{K}/\text{J}]^{\text{gas}}$ as:

$$[\text{K}/\text{J}]^{\text{gas}} = \log \frac{\sum_{i=1}^{n_p} K_i M_i^{\text{gas}}}{\sum_{i=1}^{n_p} J_i M_i^{\text{gas}}} - \log(\text{K}/\text{J})_\odot \quad (1)$$

where n_p is the total number of gas particles belonging to a GLO, M_i^{gas} the hydrogen remnant in the i^{th} particle, K_i and J_i their chemical abundances, and $(\text{K}/\text{J})_\odot$ the cor-

responding solar abundance ratio. Similar estimations can be defined for stars by summing up over the stellar populations. These analysis provides us with information on the metallicity distribution of the gaseous and stellar components in each galactic system as a function of z . It has to be noted that in these models we are not able to distinguish between ionized and neutral gas, therefore we assume that both phases have the same chemical abundances.

3.2 Simulated DLAs

Observations of DLAs provide information on the chemical properties of the H I components belonging to structures lying along LOSs towards QSOs. Specifically, DLAs are defined as those H I components with column density $N(\text{H I})$ higher than $2 \times 10^{20} \text{ atoms cm}^{-2}$ (Wolfe et al. 1986). In the simulations, the H I components of the main baryonic clump (i.e., the GLO) within the virial radius of the galactic object will be considered as possible absorbers. Following Tissera et al. (2001), we use Monte Carlo technique to draw LOSs through GLOs and estimate the chemical properties of the H I components with $N(\text{H I}) > 2 \times 10^{20} \text{ atoms cm}^{-2}$ along them. For each LOS drawn through a GLO at a certain z we estimate the chemical abundances of the H I component along it by applying Eq.1., but where the sum is now defined over the particles which are situated along a given LOS. Three different DLA mock catalogs have been produced by generating three different random observers and drawing a LOS through each GLO from each of the three observers. In this way, we generated a total of 380 DLAs distributed between $z = 0.26$ and $z = 2.3$.

Owing to geometrical considerations, random LOSs tend to map with higher probability the properties of the outer regions of the absorbing systems, missing information coming from the central regions (e.g., Jimenez et al. 1999; Somerville et al. 2001; Savaglio 2000). Note that impact of geometrical effects depends on the absorber redshift as we will discuss later on. It still remains to be answered how representative of the properties of their hosting structures these observations are (e.g. Pettini 2003). This is one of the aims of this paper since the simulations provide information on both the DLA system and its host galaxy.

For this purpose, we estimate the impact parameter b in kpc as a function of z . The b parameters found in the simulations take values from few up to ≈ 60 kpc with a mean of ≈ 15 kpc, again showing the fact that random LOSs tend to map preferentially the outer regions of the baryonic main clumps. We found that for the absorbers at $z < 1$, the percentage with $b \leq 5$ kpc is 39% of the total, while at $z > 1$ this percentage goes down to 21%. In terms of the virial radius, we found that regions causing the absorptions are between 5% to 25% of the virial radius of the galactic objects. This result is in marginal agreement with that reported by Haehnelt et al. (2000), but it is roughly consistent with the expected scale-length of a centrifugally supported disk if the specific angular momentum of baryons is assumed to be conserved during disk formation. This difference found between the results of Haehnelt et al. and ours may be due to the fact that our simulations include star formation. The transformation of gas into stars has non-negligible effects on the gas dynamics, specially during violent events as reported by Mihos & Hernquist (1996) and Domínguez-Tenreiro, Tis-

sera & Sáiz (1998), among others. We also detect a slight trend for this average percentage to increase with z .

4 METALLICITY EVOLUTION

In this Section we analyse different statistical moments of the metallicity of the ISM and the associated SPs intercepted by random LOS. We will analyse the variation of unweighted and mass-weighted means of different abundances with redshift. We will also apply linear regression through the data to quantify possible evolutionary signal. The mass weighted mean abundances as a function of redshift provide clues on the global metallicity content of the Universe, while linear regressions through the data or unweighted means give idea on the changes in the chemical abundances of the individual galactic objects.

The chemical elements more commonly used to assess the metallicity properties of DLAs are zinc (Zn) and iron (Fe). The Zn is usually considered a reliable tracer of metallicity since it is weakly depleted onto dust. However, its poorly understood nucleosynthesis and the difficulty to be detected at low metallicity make this element troublesome to interpret. On the other hand, the Fe is heavily depleted onto dust grains but it is less biased than Zn against low metallicity DLAs, and its nucleosynthesis is well understood.

The so-called α -elements (e.g., silicon (Si), sulphur (S), calcium (Ca), oxygen (O)) are also observed in DLAs although some of them could be importantly affected by dust depletion. The dust-to-gas ratio is larger for refractory elements and varies with environment making corrections complicated (Vladilo 2002). The simulated sample is not affected by dust depletion or obscuration, neither it is biased against low or high metallicity column densities, hence these simulations are a powerful tool to explore the nature of DLAs.

In order to properly confront our results with observations, we have gathered the available observational data of DLAs within our redshift range of interest and applied to them the same analysis performed to the simulated DLAs. We have chosen to use the data provided by Vladilo (2002) since they include self-consistent dust corrected values making them more suitable to constrain the results obtained from our simulations which do not include dust effects. This observational sample includes data from several authors and, in particular, overlaps with the data base analysed by Prochaska & Wolfe (2002).

4.1 The Interstellar Medium

For the purpose of assessing possible signals of global or intrinsic evolution through the comparison of means at different redshift intervals (e.g., Prochaska & Wolfe 2000), we split both the observed and simulated samples into two redshift bins: $z_{\text{low}} = [0.25, 1.5]$ and $z_{\text{inter}} = (1.5, 2.35]$. Following Tissera et al. (2001), we first estimate at each analysed z the unweighted mean $\langle [X/H] \rangle = 1/n \sum_n [X/H]$ for Zn, Fe and Si abundance ratios (represented by X in the previous equation) for the H I along the LOSs intercepting the GLOs (where n is the number of LOSs at a given z). The $\langle [Zn/H] \rangle$ and $\langle [Fe/H] \rangle$ values at each z are shown in Fig.1 as filled circles with error bars indicating 1σ standard deviations. Regarding the dispersions in the simulated DLAs sample,

we found that they are comparable to the dust corrected data from Vladilo (2002) as it can be also appreciated from Fig.1. Table 1 summarizes the observed estimations for the data presented by Vladilo (2002) ($\sigma_{z_{\text{low}}}^{\text{obs}}, \sigma_{z_{\text{inter}}}^{\text{obs}}$) and those corresponding to the simulated DLAs ($\sigma_{z_{\text{low}}}^{\text{sim}}, \sigma_{z_{\text{inter}}}^{\text{sim}}$)

We will refer to the difference between the unweighted means of a given abundance ratio ($[X/Y]$) estimated for the simulated DLAs at the two adopted redshift intervals as $\Delta\langle[X/Y]^{\text{sim}}\rangle_{\text{u}}$. In the case of $[Zn/H]$, the difference $\Delta\langle[Zn/H]^{\text{sim}}\rangle_{\text{u}}$ yields an intrinsic evolution of -0.23 ± 0.09 dex for the simulated DLAs. A linear regression through the simulated sample gives an anti-correlation signal with a slope of $d\log[Zn/H]/dz = -0.26 \pm 0.04$ dex. In both cases, errors have been estimated by using the re-sampling bootstrap technique with 500 random samples. Estimates of the unweighted mean $\langle[Fe/H]^{\text{sim}}\rangle_{\text{u}}$ at low and intermediate redshift bins and a linear regression show an intrinsic evolution in the simulated sample of $\Delta\langle[Fe/H]^{\text{sim}}\rangle_{\text{u}} = -0.33 \pm 0.11$ dex, and $d\log[Fe/H]/dz = -0.36 \pm 0.05$ dex, respectively. The linear regressions trough the $[Zn/H]$ and $[Fe/H]$ abundance ratios for the whole sample of simulated DLAs are depicted in Fig.1.

Table 1 summarizes the linear regressions obtained for the simulated and observed DLAs with and without dust corrections. Table 2 gives the differences between the unweighted means estimated at the two adopted redshift bins for different abundance ratios obtained from the simulated DLAs ($\Delta\langle[X/Y]^{\text{sim}}\rangle_{\text{u}}$). This table also shows the corresponding values for the observed DLAs reported by Vladilo (2002) with and without dust corrections ($\Delta\langle[X/Y]_{\text{dust}}^{\text{obs}}\rangle_{\text{u}}$ and $\Delta\langle[X/Y]^{\text{obs}}\rangle_{\text{u}}$, respectively).

The cosmic mean metal evolution can be estimated by calculating the difference of H_I mass weighted averages at the low and intermediate redshift bins ($\Delta\langle[X/H]^{\text{sim}}\rangle_{\text{w}}$). These estimations yield an evolution of 0.51 ± 0.39 dex, 0.85 ± 0.48 dex and 0.72 ± 0.59 dex for the $[Zn/H]$, $[Fe/H]$ and $[Si/H]$, respectively (bootstrap errors given, BE). Note that although the values are large, the BE errors indicate that they are statistically consistent with non-evolution within $2\sigma_{\text{BE}}$. Table 3 summarizes these differences for both, simulations and observations.

Overall, we acknowledge higher evolution signal in our simulated DLA sample than that obtained from the dust-corrected sample of Vladilo (2002), although the bootstrap errors of the observations are quite high suggesting that the sample suffers of low statistical number. We will come back to this point in Section 5.

4.2 Stellar Populations

DLAs are H_I clouds detected in absorption providing no direct information on the SPs associated to the absorber. One of the advantages of our models is that we can compute the metallicity properties of the stars situated along the LOSs.

In this case, we find an intrinsic evolution signal of 0.23 ± 0.13 dex (BE) for the $[Zn/H]$, 0.16 ± 0.13 dex for the $[Fe/H]$ and 0.15 ± 0.17 dex for the $[Si/H]$, over the z -range of interest. In Fig.2, we plot the unweighted mean abundance ratios at each analysed redshift (filled circles) and the dust-corrected data of Vladilo (2002; open pentagons).

We also define the stellar mass weighted mean metal-

licity of the SPs along LOSs. The difference between these mean values at the low and intermediate redshift bins indicates a global evolution of 1.00 ± 0.48 dex (BE), 0.84 ± 0.34 dex and 0.92 ± 0.57 dex for the $[Zn/H]$, $[Fe/H]$ and $[Si/H]$, respectively.

The degree of intrinsic and global evolution detected in the simulated SPs and the ISMs are comparable (within $2\sigma_{\text{BE}}$) suggesting that both mass components reflect similarly the rate of enrichment of the galactic objects as they evolve. In order to quantify if they have the same amount of enrichment, we calculated the difference between the SP abundances and those corresponding to the gaseous component along each simulated LOS. For the unweighted means, we found that stars are always less metal-rich by, on average, ≈ 0.50 dex (≈ 0.40 dex for $[Zn/H]$ and ≈ 0.70 dex for $[Fe/H]$) than the ISM where they inhabit at any redshift, while the weighted means are very similar. These results indicate that, in these models, there are stellar populations that have lower metallicities compared to those of their associated DLAs, but represent a small percentage of the total stellar mass; while a larger fraction of stars is as metal rich as the ISMs they are embedded in, at both redshift intervals. It is very interesting to note that the importance of this segregation in the abundances of the SP and the ISM identified along random LOSs depends on the chemical element considered. The so-called α -elements show a smaller difference than those mainly produced by SNIa. The difference is originated in the distinct star formation histories of the regions and the time delay between the two kind of SN events (Tissera et al. 2002).

Finally, we find that the dispersions of abundances of the SPs are higher than those measured for the ISMs (see Table 1) along LOSs, showing that abundances of stars in regions mapped by those LOSs are more heterogeneous (for example, the $[Fe/H]$ show $\sigma_{z_{\text{inter}}} = 0.74$ and $\sigma_{z_{\text{low}}} = 0.85$, and for $[Si/H]$ we have $\sigma_{z_{\text{inter}}} = 0.66$ and $\sigma_{z_{\text{low}}} = 0.70$).

The simulated abundances and their dispersions are a consequence of the variety of GLOs with different evolutionary histories. The fact that their ISMs when mapped by random LOSs show similar chemical properties to those measured in DLAs supports the hypothesis that DLAs absorptions can be actually produced by a mixture of galaxy types. Since we are simulating typical field regions of the Universe, the majority of the GLOs are supposed to represent typical spirals at $z = 0$ with some contributions from other morphological types (Dressler 1999). As we go to higher z , the substructures that have merged to form them start to emerge as separate entities. The mixture of the properties of these progenitor objects gives rise to the chemical characteristics of the simulated absorption clouds and the SPs.

5 DEPENDENCE OF METALLICITY ON COLUMN DENSITY

There is evidence showing that high metallicity and high column density DLAs are missing from the observational data. However, it is not clear if this is owing to the depletion of metals onto dust from the diffuse phase, to geometrical effects, or if they are not present at all in nature. Boissé et al. (1998) estimated an observational region where all observed DLAs lay, defined as $F = [Zn/H] + \log N(H_I)$ with

$18.8 < F < 21$. In order to mimic in the models the observational lack of high metallicity and high column density DLAs, we followed Prantzos & Boissier (2000) and applied this observational filter to the simulated sample. We found that 30% of the sample is cast out, with 19% having $F > 21$. These DLAs are high metallicity and high column density absorbers.

Estimations of the evolution signals for the filtered simulated DLAs sample indicate that both intrinsic and global evolution are much weaker than those obtained from the original simulated sample, as it can be seen from Tables 1, 2 and 3. The difference of unweighted means for the filtered sample are $\Delta\langle[\text{Zn}/\text{H}]_{\text{fil}}^{\text{sim}}\rangle_{\text{u}} = -0.03 \pm 0.09$ dex, $\Delta\langle[\text{Fe}/\text{H}]_{\text{fil}}^{\text{sim}}\rangle_{\text{u}} = -0.21 \pm 0.08$ dex and $\Delta\langle[\text{Si}/\text{H}]_{\text{fil}}^{\text{sim}}\rangle_{\text{u}} = -0.19 \pm 0.08$ dex, while for the mass weighted means are $\Delta\langle[\text{Zn}/\text{H}]_{\text{fil}}^{\text{sim}}\rangle_{\text{w}} = -0.14 \pm 0.04$ dex, $\Delta\langle[\text{Fe}/\text{H}]_{\text{fil}}^{\text{sim}}\rangle_{\text{w}} = -0.24 \pm 0.21$ dex and $\Delta\langle[\text{Si}/\text{H}]_{\text{fil}}^{\text{sim}}\rangle_{\text{w}} = -0.27 \pm 0.09$ dex. We have also carried out estimations of evolution by applying only the upper limit of the observational filter finding very similar results. Hence, the high column density and high metallicity DLAs are the ones imprinting signals of intrinsic and global evolution.

The physical processes that cause the non-detectability of such HI clouds remains to be explained. Although dust can account for it as it has been reported by several authors (e.g., Hou et al. 2001), recent results from a study of DLAs against radio-selected QSOs (Ellison et al. 2001) suggest that dust may not be as important as previously thought since high column density DLAs have not been detected yet in this sample. In the simulations we found that the percentage of DLAs with these characteristics (i.e., outside the upper limit of the observed filter) is only 3% and 16% at $z > 1$ and $z < 1$, respectively. Hence, according to our results, the radio-selected sample is still small to discard geometrical effects as a possible cause, since most observed DLAs are at $z > 1$ (Cen et al. 2003). Moreover, because the filtered simulated DLAs are more consistent with the dust-corrected sample, our findings do not support the hypothesis that this upper observational limit is caused by dust obscuration but they favour geometrical effects¹.

We can use the simulations to explore the characteristics of DLAs cast out by the filter. In Fig.3, we plot the stellar mass along the LOSs versus the filter F . The dashed-dotted lines depict the limits established by the observational filter. Stellar populations associated to DLAs have been represented by filled triangles. Sub-DLAs ($10^{19} < N(\text{H}_I) < 2 \times 10^{20}$ atoms cm^{-2}) have been also included in this figure but they will be discussed in Section 7. As it can be seen from the distribution of the filled symbols, there is a clear correlation between the stellar mass associated with a given DLA and the filter characteristics of that DLA. There are very few DLAs with $F < 18.8$, and all simulated

DLAs with $M_{\text{stars}} > 10^8 M_{\odot}$ have $F > 21$. Therefore, in our models, this observational filter directly translates into a stellar mass cut-off. As it has been shown, most LOSs map the external regions of DLA galaxies. However those with $F > 21$, which are comparable to those missing from observations, have impact parameters $b < 5$ kpc. Hence, LOSs with $M_{\text{stars}} > 10^8 M_{\odot}$ intercept the central regions. Although the percentage of such LOSs is low ($\approx 7\%$ of the total), it is enough to imprint global evolution with redshift in our simulations. It has been already mentioned that simulated DLAs with low impact parameters are more common at $z < 1$ because of geometrical effects. These results suggest that some effort should be devoted to enlarge the sample of observed DLAs at low redshift since it could be profitable in order to test the existence of DLAs with high $N(\text{H}_I)$ and high metallicity. Yet, another possibility could be that the gas densities might have been lowered down by SN energy injection (not treated in this work), and consequently DLAs with these features are not present at all in nature as suggested by Ellison et al. (2001).

6 THE α -ELEMENTS

The abundance ratios of the so-called α -elements (i.e., Si, S, C, O) in DLAs have been subject of many studies (e.g., Lu et al. 1996; Pettini et al. 1997; Pettini et al. 2000) because they are thought to be good indicators of the SF history of DLA galaxies. This argument is based on the fact that the abundance patterns of the α -elements in the Milky-Way show enhancement for metal poor stars ($[\alpha/\text{Fe}] = +0.5$ dex at $[\text{Fe}/\text{H}] \leq -0.66$) and then, a decline towards solar values for higher metallicities. This change of behaviour can be explained by taking into account the time-delayed contribution of SNIa to the chemical enrichment of the ISM. This type of SNe are the main producer of Fe which is ejected into the ISM after a time-delay equal to the life-time of the binary systems from which they arise (Thielemann et al. 1993). The timing of these chemical contributions are determined by the particular history of star formation of each galaxy.

It has been found that the presence of dust in DLAs affects the determinations of $[\alpha/\text{Fe}]$ ratios in a complicated way. Estimations of dust-corrected abundances yield nearly solar values (Vladilo 1998; Vladilo 2002). Recently, Ellison & López (2001) found a pair of DLAs selected via radio observations which show solar and sub-solar $[\alpha/\text{Fe}]$ abundances. Sub-solar values would suggest that the H_I clouds have been mainly chemically enriched by SNIa. Based on the discussion presented by Vladilo (1998) and Hou et al. (2001), among others, we focus on the comparison of our results with dust-corrected observations since metal depletion onto dust has not been considered in our simulations.

First observational results of $[\alpha/\text{Fe}]$ in DLAs shown some enhancements and a lack of trend with increasing redshift and metallicity (Pettini et al. 1997). However, recently, a behaviour consistent with a general trend for decreasing α -enhancement with metallicity has been reported by Centurión et al. (2000), Molaro et al. (2001) and Vladilo (2002). In particular, Molaro et al. (2001) estimated a change of -0.36 dex from a regression analysis of $[\text{S},\text{O}/\text{Zn}]$ providing the first results that give hints on metallicity evolution in the α -elements. In a DLA sample with redshifts

¹ An alternative option is proposed by Schaye (2001b) who claims that the maximum H_I column density is determined by the conversion to molecular hydrogen. The fraction of molecular H correlates with dust content and total hydrogen, and anticorrelates with the intensity of the incident UV radiation. However, this author does not discard dust effects as the possible explanation of the apparent lack of systems with low column density and high metallicity which cannot be accounted for by his models.

> 1.5 , Prochaska & Wolfe (2002) found that dust can affect strongly the measurements in those absorbers with $[\text{Si}/\text{H}] > -1.5$. They found that DLAs at low metallicity, which can be considered dust-free, have significant α -enrichment, as indicated by the $[\text{Si}/\text{Fe}]$ values which exhibit a plateau of ≈ 0.3 dex at $[\text{Si}/\text{H}] < -1.5$ dex. The increase in $[\text{Si}/\text{Fe}]$ at higher values of $[\text{Si}/\text{H}]$ can be explained by dust depletion. Thus, when allowing for this effect, these authors found that the abundances of different systems are quite homogeneous.

In Fig.4(a) we show the distribution of $[\text{Si}/\text{Fe}]$ versus $[\text{Fe}/\text{H}]$ for the simulated DLAs, the dust-corrected data of Vladilo (2002). We can see that the abundance ratios for the simulated DLAs take values from solar up to $[\text{Si}/\text{Fe}] \approx 0.30$ dex, in very good agreement with the observed dust-corrected abundances. Note also that there are some simulated DLAs with low metallicities and (sub)solar $[\text{Si}/\text{Fe}]$, indicating a main enrichment by SNIa. This behaviour is consistent with that reported by some observations (Ellison & López 2001) which show sub-solar α values for some low metallicity absorbers, and has arisen from the natural evolution of the GLOs which takes into account infall of material from the dark matter halo as well as inflows within a given GLO. In order to assess the presence of evolution of the α -elements with metallicity, we performed a linear regression through the simulated DLA data finding -0.15 ± 0.01 dex from $[\text{Si}/\text{Fe}]$ values. These estimations have been performed with those simulated DLAs that satisfy the usual definition of $N(\text{H}_I) > 2 \times 10^{20}$ atom/cm².

In Fig.4(b), we have plotted the DLAs that are within the observational filter defined in the previous Section. Note how the filter tends to cast out the simulated DLA at the plateau of the relation, resulting in a better agreement with observations: $d\log[\text{Si}/\text{Fe}]/d[\text{Fe}/\text{H}] = -0.23 \pm 0.01$ dex. This effect is caused because the observation filter casts out the high metallicity and high column density H_I clouds but by using the $[\text{Zn}/\text{H}]$ abundance as an indicator of metallicity. This element is produced by SNII and has a different ejection timescale than Fe which is mainly produced by SNIa. This different timing between the two ejecta types can produce clouds with different relative enrichments (Tissera et al. 2002).

Finally, Fig.4(c) shows the unweighted mean $\langle[\text{Si}/\text{Fe}]\rangle$ of the simulated DLAs at each analysed z as a function of the metallicity given by the corresponding unweighted mean $\langle[\text{Fe}/\text{H}]\rangle$, where the error bars represent the standard dispersions. As it can be appreciated from this figure, the dispersions for the $\langle[\text{Fe}/\text{H}]\rangle$ at each redshift are very large and more important than those of the $\langle[\text{Si}/\text{Fe}]\rangle$ (Prochaska & Wolfe 2002). Hence, while absorbers have more homogeneous $[\alpha/\text{Fe}]$ abundances at a given redshift, they show very different Fe content. This is the result of their different histories of evolution and star formation which determined the timing between SNIa and SNII contributions to the ISM.

Another way of assessing the differential enrichment by SNII and SNIa is by analyzing the evolution of $[\text{Si}/\text{Fe}]$ as a function of redshift (Fig.5). As it can be seen, the agreement with the dust-corrected data from Vladilo (2002) is very good, in the amount of enrichment, dispersion and trend. A linear regression through the simulated data yields $d[\text{Si}/\text{Fe}]/dz = 0.05 \pm 0.01$ dex (0.04 ± 0.01 dex for the filtered sample). The positive correlation is due to the increase of

Fe content as the stellar populations get older and start to produce SNIa.

Finally, in Fig.6 we plot the $[\text{Si}/\text{Fe}]$ ratio as a function of the metallicity $[\text{Fe}/\text{H}]$ for the ISM and SP of DLAs and Sub-DLAs; the discussion of the later ones is postponed till the next Section. Regarding the α -enhancement of the SPs associated to DLAs (filled stars), we can see that their $[\text{Si}/\text{Fe}]$ abundances are higher than the corresponding ISM and most of them formed in the higher α -content levels, implying that the regions mapped by the random LOSs are those that have experienced a burst of SF after which the SF activity has proceeded in a more quiet way (see Tissera et al. (2002) for an analysis of the age of the stellar population in DLA systems). This fact is also the cause of having a SP less rich in Fe than their ISM along the LOSs, since as the gas is enriched by SNIa from the old SP, on average, no important star formation locks this material into stars. The α -content of the SPs does not show any trend contrary to their ISMs as mapped by DLAs.

6.1 Brief discussion on the meaning of the statistical analysis

In this paper we have applied the two commonly used statistics to assess evolution in the metallicity content of H_I clouds: differences of means at different redshifts and linear regressions. These two statistics have been applied to the simulated DLAs and the observational data presented by Vladilo (2002). A close inspection of these results presented in Tables 1, 2 and 3 reveals interesting features that we would like to discuss. We have chosen to show the bootstrap errors which give an indication of the statistical significance of the relations, but, the standard dispersions in simulated and observed DLAs are high (Table 1), making difficult to extract clear results.

Let us first look at the observations. This analysis is focused on the $[\text{Fe}/\text{H}]$ ratio, since iron is much more affected by dust depletion than other chemical elements. The differences $\Delta\langle[\text{Fe}/\text{H}]^{\text{obs}}\rangle_{\text{u}}$ and $\Delta\langle[\text{Fe}/\text{H}]^{\text{obs}}\rangle_{\text{w}}$ for the observed DLA sample without dust correction are pretty similar, showing negligible evolution both for unweighted and mass weighted means. When dust corrections are incorporated, the evolution shown by the unweighted means remains almost unchanged, while the difference between mass weighted means increases to $\Delta\langle[\text{Fe}/\text{H}]_{\text{dust}}^{\text{obs}}\rangle_{\text{w}} = -0.30 \pm 0.35$ dex. However, this value cannot be considered as indicative of the presence of some evolution because of its large error. This lack of evolution is consistent with the negligible signal found by Prochaska et al. (2002) when applying these two different statistics to a DLA sample that covers a redshift interval twice as large than the one considered in the present work.

However, when considering the slope obtained from the linear regression through the observations, we found a more statistical significant signal for intrinsic evolution, $d\log[\text{Fe}/\text{H}]/dz = -0.17 \pm 0.11$ dex, which increases to -0.31 ± 0.14 dex, when dust corrections are applied. These values are pretty similar to those obtained by Vladilo (2002) from the analysis of these data on a larger redshift range. Hence, we obtained different results for the metal evolution in the observed sample, specially for the intrinsic evolution, depending on which statistics is applied.

A similar behaviour is detected for the simulations,

where more statistically significant signals are found when linear regressions are used. As it can be appreciated from Fig.1 and Fig.5, [Zn/H], [Fe/H] and [Si/Fe] ratios for both simulated and observed DLAs have increasing dispersions with redshift, leading to a picture that looks likely triangular. In the simulations, this shape is caused by the combination of enrichment of the ISM of the building blocks and the continuous gas infall which gives rise to metallicity gradients. These gradients caused the large abundance dispersions detected in the simulated DLAs, since random LOSs mapped different regions of the building blocks (see Section 8). The high metallicity and high column density simulated DLAs help to increase continuously the upper enveloped abundances of the triangle, this is why the filtered simulated sample shows less evolution when evaluated by differences of means. However, for the linear regressions the DLAs cast out by the filter are too few to actually change the general trend. Finally, the fact that the filtered sample reproduces the dust-corrected observed trends provides evidences for the upper limit of the observational filter not to be determined by dust absorptions.

7 THE IMPACT OF SUB-DLAs

Recent observational results of low density H_I clouds along LOSs, the so-called sub-DLAs, obtained by Péroux et al. (2001, and references therein) show that clouds with $N(\text{H}_I)$ in the range $10^{19} - 2 \times 10^{20} \text{atom cm}^{-2}$ contribute with an important fraction of the neutral gas of the Universe, specially at $z > 3.5$.

Sub-DLAs are associated with regions of lower stellar-mass content than DLAs, as it is shown in Fig.3. However, we find sub-DLAs to have a negligible contribution to the global metallicity evolution of the simulated box since in our models, such evolution is mainly driven by the high metallicity and high column density H_I clouds. If sub-DLAs are incorporated to our calculations, we find that they affect the estimation of the intrinsic evolution making the signal even more stronger for both the gas and the stellar population. Hence, in the redshift range studied in this work, sub-DLAs seem to have no impact on the estimation of chemical evolution of the Universe but they should be taken into account to study the evolution of the chemical properties of the ISM and SP in DLA galaxies.

In fact, if sub-DLAs are included in the estimations of [Si/Fe] versus [Fe/H] the metallicity evolution signal is even clearer, and an abundance pattern similar to that observed in the Milky-Way is identified in the distribution as it can be seen in Fig.6. In the case of the filtered sub-DLA/DLA sample we found metallicity evolution of -0.29 ± 0.03 dex (BE). The stellar populations associated to sub-DLAs tend to show mild α -enhancement and the total filtered sample shows weak evolution with metallicity: 0.07 ± 0.03 dex (BE).

The following step would be to disentangle if sub-DLAs are mainly associated with small objects or with the very outskirts of DLA galaxies. Firstly, we probed for a dependence of the $N(\text{H}_I)$ with the virial velocity of the associated DLA galaxies finding that DLAs and sub-DLAs are thrown out from a similar mixture of galactic halos with no dependence on virial velocity. Secondly, we looked at the relation between the impact parameter b and $N(\text{H}_I)$ (Fig.7). A clear

trend is found for the higher impact parameters to be mainly associated with sub-DLAs. Note that sub-DLAs also trace the intermediate regions ($5 \text{ kpc} < b < 8 \text{ kpc}$). Although this correlation is already well-known, we have estimated it in order to show that these model and simulation are able to reproduce them.

According to these results, both DLAs and sub-DLAs could be tracing the ISMs of the same DLA galaxies with sub-DLAs providing more information on the outskirts of the galactic objects. However we note that, in our models, we may be overestimating the gas column densities and consequently, underestimating the impact parameters due to the well-known problem of excessive angular momentum transfer from baryons to the dark matter component. However, this effect works in the sense of erasing the low density region contributions by making the objects more concentrated with their gas density artificially higher in the centre. Hence, the fact that we get a signal of this kind suggests that this could be a real physical effect. In that case, sub-DLAs should be included in the analysis of the chemical evolution of the ISMs.

Finally, stars associated with sub-DLAs show α -enhancement (Fig.6(b)), suggesting that the low-metallicity population in the galaxies such as the Milky-Way, could have been formed in the outer and intermediate regions of protogalactic objects. Note that our results do not imply any constrain on the mass of such protogalaxies, actually we find no dependence at all on the virial mass.

Ionized gas may be significant in systems with low $N(\text{H}_I)$ which can be much more affected by ionization radiation (Viegas 1995). Thus, the analysis of sub-DLAs should be taken only as indicative since, in our model, the chemical abundances were obtained by assuming all gas in neutral phase.

8 DLA GALAXIES

In this Section we focus on the analysis of host galaxies of the simulated DLAs. All the galactic systems analysed have been resolved numerically with more than 2000 particles within their virial radius and with a spatial resolution of 1.5 kpc. A detail description of these simulated galaxies has been presented in Section 3.1.

Recent observations have improved the statistics of DLA galaxies (Rao & Turnshek 2000; Nestor, Rao & Turnshek 2001), although it is still difficult to assert which sort of systems are responsible for the absorption features in the spectra of QSOs at different redshifts. There are now approximately 10 DLA galaxies observed at $z < 1.65$ (Le Brun et al. 1997; Rao & Turnshek 2000). These observations show systems with different morphologies and luminosities including a significant number of dwarf and low surface brightness galaxies, albeit also spirals. Turnshek, Rao & Nestor (2001) compared properties of these DLA galaxies with those of local galaxies. We will use this observations to confront with the properties of the GLOs which host the simulated DLAs.

Our model allows to estimate the magnitudes of the GLOs in different wavelengths by using population synthesis model (Tissera et al. 1997) such as GISSEL 98 (kindly provided by G. Bruzual). For each SF episode we estimate the flux distribution according to its age and metallicity.

Then, we sum up the contribution of all SPs belonging to a GLO at a certain redshift in order to estimate its total luminosity. In Fig.8, we plot the blue absolute magnitude of the GLOs at $z \leq 1$, distinguishing between those that are within (filled circles) and outside (open circles) the observational filter. Sub-DLAs have been included for completeness. From this figure we observe that those GLOs which give origin to DLAs/sub-DLAs within the observational filter show a trend with magnitude similar to that found by Turnshek et al. (2001) for both DLAs and local galaxies, in the sense that the brighter the galaxies, the larger the impact parameter of the associated DLA. The inclusion of GLOs cast out by the observational filter tend to erase the correlation signal because the small b , which are mainly related to DLAs with high metallicity and high H_I column density, are associated to galaxies of any luminosity; while larger impact parameters are related to the brighter GLOs.

We also estimate the total blue luminosity of GLOs at different z . As it can be appreciated from Fig.9, most of the building blocks producing the absorptions have $(L/L^*)_B < 0.5$ as shown by the median at each z (filled circles), in agreement with observed DLA galaxies at $z < 1$. The dispersion found in the simulated ratios agrees well with the observed fact that DLA galaxies cover a large range of luminosities. We also found a trend for DLA galaxies to increase their typical luminosity with redshift. Note however that numerical resolution could affect this last result.

The information on the chemical properties of the ISMs and the SPs provided by the LOSs suggests that the simulated DLA galaxies at different redshifts have metallicity gradients. In order to assess how fairly random LOSs properly sample the chemical properties of the DLA galaxies, we estimate the abundances of the ISMs and SPs in each GLO in concentric shells as explained in Section 3.1. We calculate averages over the abundances within each shell in GLOs at each analysed z .

Fig.10 shows the mean values over GLOs as a function of z for the concentric shells with inner radius varying from $r = 0$ kpc to $r = 10$ kpc and the outer one fixed at $r = 2R_{\text{opt}}$ (i.e., the estimations at $r = 0$ implies that all the mass associated to the simulated galaxies has been taken into account). As it can be seen from this figure, the gas in the external regions is less metal enriched than the material in the central areas confirming the existence of metallicity gradients in the ISM of GLOs at all redshifts. Linear regressions through the simulated data yield evolution signal in the chemical content of the ISM of the whole GLOs (i.e., $r > 0$ kpc) and of the ISM outside the very central regions (i.e., $r > 3$ kpc) of -0.32 ± 0.06 dex (BE) and -0.23 ± 0.03 dex (BE) for $[\text{Fe}/\text{H}]$ (similar trends have been found for $[\text{Zn}/\text{H}]$). This estimation agrees with that obtained from the linear regression of the simulated DLAs. For the ISM at $r > 6$ kpc and $r > 10$ kpc we get -0.26 ± 0.20 dex (BE) and -0.07 ± 0.26 dex (BE), implying that statistically, there is no evolution in the metal content of the intermediate and external regions of the galactic structure, in agreement with the filtered simulated DLAs. According to these results we predict that the observed global metallicity of the DLA galaxies might be underestimated, since random LOSs tend to map the external regions, and no global evolution would be detected unless central areas are taken into account.

A similar analysis has been carried out for the SPs

within each shell finding that stars in the outer parts are less metal-rich than those in the inner regions (Fig.11). Note that stars with $r < 6$ kpc are the ones pulling up the averages to nearly solar values. In this case, the gap between the metallicity of stars in the inner regions and that of the rest of the GLOs is larger than those of the ISM, where there is a continuous decrease of metallicity with radius. Stars in the outer regions also show higher α -abundances as expected. We stress the fact that in the GLOs there are primordial stars with very low Fe content ($[\text{Fe}/\text{H}] < -3$) and high α -enhancements but when averages are estimated, higher metallicity SPs are more massive and dominate the estimations. Finally, note that the mean abundances of the SP of the whole systems (i.e., inner radius $r = 0$) are higher than those corresponding to the ISM. This is reflecting the fact that in hierarchical clustering scenarios there is a continuous infall of pristine material from the galactic halo and that stars tend to form in the higher density regions where the metallicity is higher.

9 CONCLUSIONS

In this work we studied the possibility that the progenitors of current normal field galaxies are DLA galaxies, host of absorbing H_I clouds in the context of hierarchical clustering, where galaxies form from the merger of smaller substructures. DLAs observations provide information on the ISM of the host objects. In our models, we have the comprehensive information of the ISM and SP of the systems, allowing the performance of a consistent study in order to obtain robust conclusions on the possible nature of DLA galaxies.

We constructed mock catalogs of DLAs by drawing random LOSs through the galaxy-like objects at different z in hierarchical clustering scenarios and compared the chemical properties of the simulated ISM when mapped by LOSs with observed DLAs. We then studied the properties of the simulated DLA galaxies and assessed at which extent random LOSs can properly extract information on both the chemical properties of the galaxies as a function of z and the global evolution of the Universe.

From our simulations, we find

- the $[\text{Fe}/\text{H}]$, $[\text{Zn}/\text{H}]$ and $[\text{Si}/\text{H}]$ ratios of the simulated DLAs to match the observational range determined by DLAs with similar dispersion. In the case of the α -elements the simulated abundances are consistent with the dust-corrected data;
- intrinsic and global evolution for $[\text{Fe}/\text{H}]$, $[\text{Zn}/\text{H}]$ and $[\text{Si}/\text{H}]$ with z . However, when the observational filter suggested by Prantzos & Boissier (2000) is applied, mild evolution consistent with observations is recovered;
- that the evolution with z is mainly driven by the high metallicity and high column density DLAs albeit these DLAs represent a small percentage of the total number of LOSs ($< 10\%$);
- α -element filtered abundances to evolve with metallicity in agreement with recent observations (e.g., Molaro et al. 2001; Vladilo 2002);
- evidences that the observational filter may not be reflecting dust absorption but other effects such as geometrical ones;

- a trend for [Si/Fe] to correlate with redshift as it is expected by taking into account the different ejecta timing of SNII and SNIa;

- sub-DLAs might be providing information on the chemical properties of the external region of DLA galaxies, but they do not affect the determination of global evolution in the metal content of the simulated box, within $0.26 < z < 2.34$;

- that the building blocks in hierarchical clustering scenarios can reproduce the magnitude-impact parameter correlation of observed DLAs for $z < 1$;

- no correlation between neither the impact parameters nor the $N(\text{H I})$ with virial velocity;

- that metal-poor stars could be forming in the outer regions of galaxies at any z and the associated ISM might be tested by sub-DLA observations.

These findings imply that the building blocks of current normal galaxies in hierarchical clustering models could be host structures responsible of the DLA and sub-DLA systems and that DLA galaxies might represent a variety of galaxy morphologies with mean luminosities increasing with respect to L^* at $z = 0$ with redshift. Despite geometrical effects, a small percentage of high metallicity and high column density $N(\text{H I})$ should be identified, unless supernova energy feedback works to lower the central gas densities. Since the chances to intercept the central regions decrease with redshift, efforts should be put on detecting them at $z < 1$. Metallicity gradients of the ISM of galaxies at different redshifts may be estimated, on average, by looking at the range of the metallicities set by DLAs and sub-DLAs. However current observations would be preferentially constraining the metallicity distribution for $r > 5$ kpc.

The observed anti-correlation between impact parameter and magnitude might be the result of the particular history of formation of each galaxy which host a DLAs or sub-DLAs. However, the observational bias related to the lack of high column density and high metallicity column density works in the sense of supporting the anti-correlation by sweeping away the very low impact parameter contributors.

Stars in the simulated DLA galaxies (i.e., galaxy-like objects) are, on average, more metal-rich at the centre and metal-poor in the outskirts independently of z . Hence at $z = 0$, a galaxy, which is the result of a merger sequence, can have old and young metal-rich (and metal-poor) stars. These findings have consequences for the understanding of the origin of the abundance pattern of the Milky-Way, since, according to our models, an important fraction of the low metallicity stars are situated in the outer ($r > 6$ kpc) regions at any redshift; stars with nearly solar values are present at any redshift, but in the central regions. Hence, according to our results, the fact that observed DLAs yield low metallicity values does not imply that the associated DLA galaxies cannot have a metal rich population. The abundance characteristics of DLAs and Sub-DLAs are the results of SNIa and SNII contributions plus gas infall. The chemical characteristics of the SPs associated with simulated DLAs are consistent with having been formed in starbursts followed by quiescent periods of SF. The fact that we always identify low metallicity stars in the outskirts and no important evo-

lution of the metallicity in these regions could be showing the action of continuous infall.

Future works will be focused on the improvement of the chemical code and the performance of simulations with higher numerical resolution.

We thank the anonymous referee for a careful reading of the manuscript and useful suggestions that helped to improve our results. We thank the Max-Planck Institute for Astrophysics for the hospitality during PBT visit where this manuscript was finished. This work was partially supported by the Consejo Nacional de Investigaciones Científicas y Técnicas, Agencia de Promoción de Ciencia y Tecnología, Fundación Antorchas and Secretaria de Ciencia y Técnica de la Universidad Nacional de Córdoba.

REFERENCES

- Barton, E. J., Geller, M. J., Kenyon, S. J., 2000, *ApJ*, 530, 660
 Boissé, P., Le Brun, V., Bergeron, J., & Deharverg, J. M. 1998, *A&A*, 333, 841
 Cen, R., & Ostriker, J. P. 1999, *ApJ*, 519, L109
 Centurión, M., Bonifacio, P., Molaro, P., Vladilo, G., 2000, *ApJ*, 536, 540
 Cora, S. A., Mosconi, M. B., Tissera, P. B., & Lambas, D. G. 2000, *Proceeding of Stars, Gas and Dust in Galaxies: Exploring the Links*, ASP Conference Proceedings. Edited by Danielle Alloin, Knut Olsen, and Gaspar Galaz. San Francisco: Astronomical Society of the Pacific, vol. 221, p.283
 Domínguez-Tenreiro, R., Tissera P., Sáiz A., 1998, *ApJ*, 508, L123
 Edmunds, M. G. & Phillips, S. 1997, *MNRAS*, 292, 733
 Ellison, S. L., Lopez, S., 2001, *A&A*, 380, 117
 Ellison, S. L., Yan, L., Hook, I. M., Pettini, M., Wall, J. V., Shaver, P. 2001, *A&A*, 379, 393
 Haehnelt, M. G., Steinmetz, M., & Rauch, M. 1998, *ApJ*, 495, 647
 Hou, J. L., Boissier, S., & Prantzos, N. 2001, *A&A*, in press (astro-ph/0102188)
 Jimenez, R., Bowen, D. V., & Matteucci, F. 1999, *ApJ*, 514, L83
 Katz N. 1992, *ApJ*, 391, 502
 Le Brun, V., Bergeron, J., Boissé, P., & Deharverg, J. M. 1997, *A&A*, 279, 733
 Le Fevre et al., 2000, *MNRAS*, 311, 565
 Lia, C., Portinari, L, Carrari, G. 2002, *MNRAS*, 339, 821
 Lu, L., Sargent, W. L. W., Barlow, T. A., Churchill, C. W., & Vogt, S. S. 1996, *ApJS*, 107, 475
 Mathlin, G. P., Baker, A. C., Churches, D. K., Edmunds, M. G., 2001, *MNRAS*, 321, 743
 Metzler C. A., Evrard A. E., 1994, *ApJ*, 437, 564
 Molaro, P., Bonifacio, P., Centurión, M., D’Odorico, S., Vladilo, G., Santin, P., Di Marcantonio, P., 2000, *ApJ*, 542, 44.
 Mosconi, M. B., Tissera, P. B., Lambas, D. G., & Cora, S. A. 2001, *MNRAS*, 325, 34
 Navarro J.F., White S.D.M. 1994, *MNRAS*, 267, 401
 Navarro, J.F., Steinmetz, M. 2000, *ApJ*, 538, 477
 Nestor, D. B., Rao, S. M., Turnshek, D. A., 2001, *Extragalactic Gas at Low Redshift*, ASP Conference Series (astro-ph/0108146)
 Nulsen, P. E. J., Barcons, X., Fabian, A. C. 1998, *MNRAS*, 301, 168
 Pettini, M., Smith, L., King, D., & Hunstead, R. 1997, *ApJ*, 486, 665
 Pettini, M., Ellison, S. L., Steidel, C. C., & Bowen, D. V. 1999, *ApJ*, 510, 576
 Pettini, M., Ellison, S. L., Steidel, C. C., Shapley, A. E., & Bowen, D. V. 2000, *ApJ*, 532, 65

- Poggianti, B., M., Smail, I., Dressler, A., Couch, W. J., Barger, A. J., Butcher, H., Ellis, R.S., Oemler, A. Jr. 1999, ApJ, 518, 576
- Prantzos, N., & Boissier, S. 2000, MNRAS, 315, 82
- Prochaska, J. X., & Wolfe, A. M. 1997, ApJ, 487, 73
- Prochaska, J. X., & Wolfe, A. M. 1999, ApJS, 121, 369
- Prochaska, J. X., & Wolfe, A. M. 2000, ApJ, 533, L5
- Prochaska, J. X., & Wolfe, A. M. 2002, ApJ, 566, 68
- Prochaska, J. X., Gawiser, E., & Wolfe, A. M. 2001, ApJ, 552, 99
- Prochaska, J. X., Naumov, S. O., Carney, B. W., McWilliam, A., & Wolfe, A. M. 2000, AJ, 12, 2513
- Rao, S. M., & Briggs, F. H. 1993, ApJ, 419, 515
- Rao, S. M., Turnshek, D. A. 2000, ApJS, 130, 1
- Ramirez-Ruiz, E., Lazzati, D., Blain, A. W., ApJL, accepted
- Salamanca, I., Kaper, L., Vreeswijk, P. M., et al. 2001, MNRAS
- Savaglio, S. 2000, Harwit, M., Hauser, M., eds., The Extragalactic Infrared Background and its Cosmological Implications, IAU, vol. 204, 24
- Schaye, J. 2001a, ApJ, 559, L1
- Schaye, J. 2001b, ApJ, 562, L95
- Somerville, R. S., Primack, J. R., & Faber, S. M. 2001, MNRAS, 320, 504.
- Thielemann, F. K., Nomoto, K., & Hashimoto, M. 1993, Prantzos, N., Vangoni-Flam, E., Cassé N., eds., Origin and Evolution of the Elements, p.299
- Thomas P. A. Couchman H. M. P., 1992, MNRAS, 257, 11
- Tissera, P. B., 2000, ApJ, 534, 636
- Tissera, P.B., Lambas, D.G., & Abadi, M.G.1997, MNRAS, 286, 384
- Tissera, P. B., Lambas, D. G., Mosconi, M., Cora, S. A., 2001, ApJ, 557, 527
- Turnshek, D. A., Rao, S. M., Nestor, D. B., ASP Conference Series, "Extragalactic Gas at Low Redshift", J. Mulchaey and J. Stocke, eds.
- Viegas, S. M. 1995, MNRAS, 276, 268
- Vladilo, G. 1998, ApJ, 493, 583
- Vladilo, G., Bonifacio, P., Centurion, M., & Molaro, P. 2000, ApJ, 543, 24
- Vladilo, G., 2002, ApJ, 569, 295
- Wolfe, A. M., Turnshek, D. A., Smith, H. E., Cohen, R. D., 1986, ApJS, 61, 249
- Wolfe, A. M., Lanzetta, K. M., Foltz, C. B., & Chaffee, F., J. 1995, ApJ, 454, 698
- Woosley, S. E., & Weaver, T. A. 1995, ApJS, 101, 181

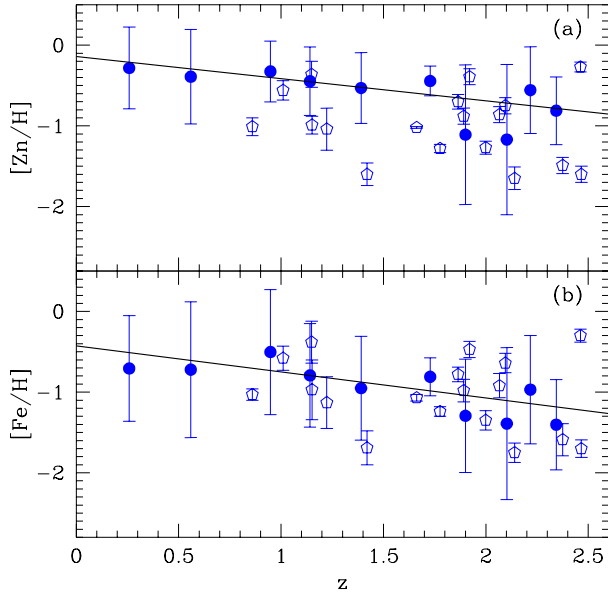


Figure 1. $\langle[\text{Zn}/\text{H}]\rangle$ (a) and $\langle[\text{Fe}/\text{H}]\rangle$ (b) unweighted mean abundances for the neutral hydrogen along the simulated LOSs with $N(\text{H}_\text{I}) > 10^{20} \text{ atoms cm}^{-2}$ as a function of redshift (*filled circles*). Error bars correspond to 1σ standard deviation. Solid lines are the least square linear regression for the whole sample of simulated DLAs. We have included the observational data of Vladilo (2002) that incorporate dust-corrections (*open pentagons*).

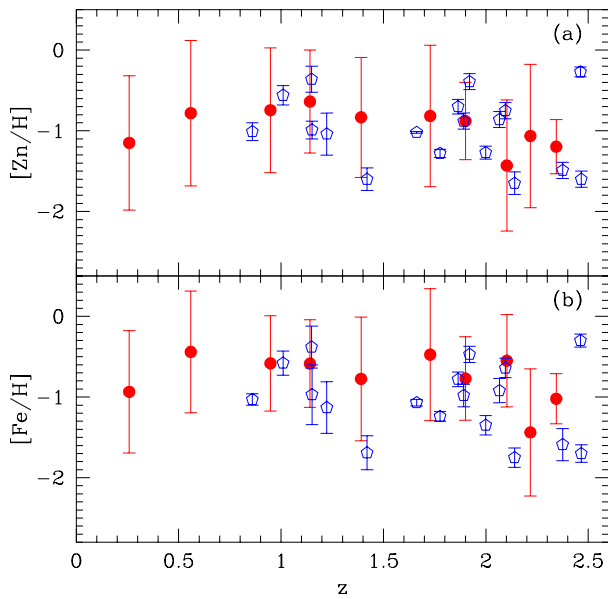


Figure 2. $\langle[\text{Zn}/\text{H}]\rangle$ (a) and $\langle[\text{Fe}/\text{H}]\rangle$ (b) unweighted mean abundances for the stellar population associated to the simulated DLAs shown in Fig.1. Abundances for dust corrected observed DLAs (Vladilo 2002) have been included for comparison (*open pentagons*).

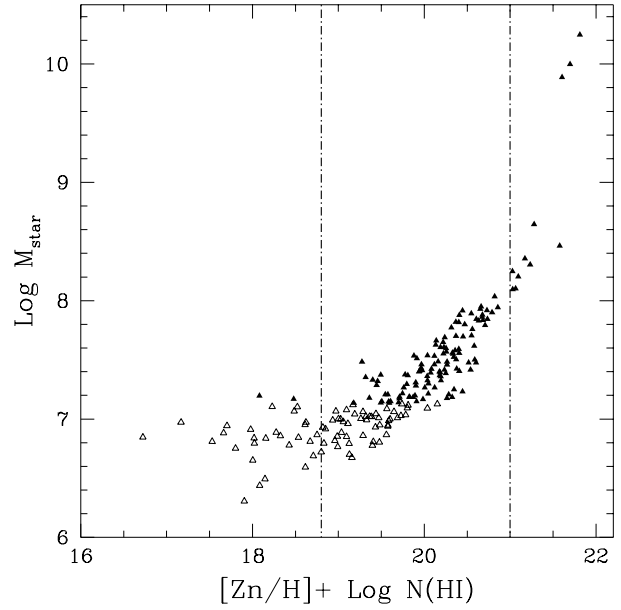


Figure 3. The stellar masses (in units of M_\odot) associated to the simulated DLAs versus the observational filter $F = [\text{Zn}/\text{H}] + \log N(\text{H}_\text{I})$, suggested by Boissé et al. (1998), for DLAs ($N(\text{H}_\text{I}) > 2 \times 10^{20} \text{ atoms cm}^{-2}$; *filled triangles*) and sub-DLAs ($10^{19} < N(\text{H}_\text{I}) < 2 \times 10^{20} \text{ atoms cm}^{-2}$; *open triangles*). The dashed-dotted lines depict the region where observed DLAs lay: $18.8 < F < 21$.

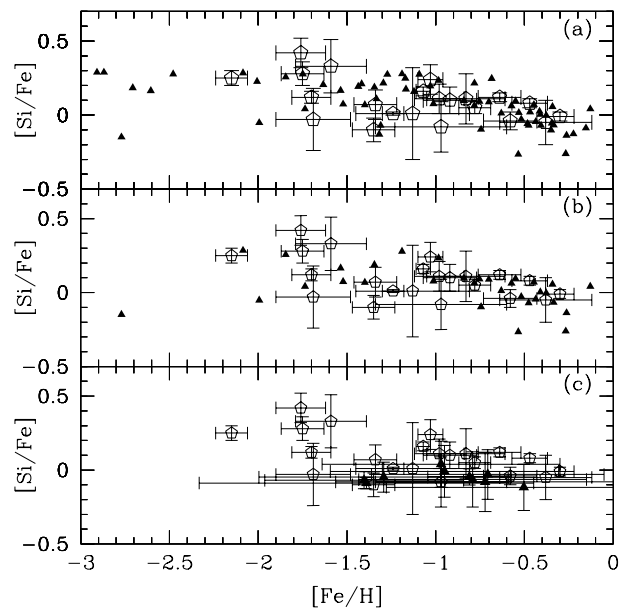


Figure 4. $[\text{Si}/\text{Fe}]$ versus $[\text{Fe}/\text{H}]$ relations obtained from simulations (*filled triangles*): a) each simulated DLA, b) each filtered simulated DLA and c) unweighted means $\langle[\text{Si}/\text{Fe}]\rangle$ and $\langle[\text{Fe}/\text{H}]\rangle$ for neutral hydrogen along LOSs for all redshifts analysed. We have included the dust-corrected observations of Vladilo (2002; *open pentagons*).

Table 1. Chemical Evolution: Linear Regressions ($LR \equiv d\log X/dz$) through observed (LR^{obs}) and simulated (LR^{sim}) DLAs (bootstrap errors given), and standard dispersions of these samples in redshift bins z_{low} and z_{inter} . For observations, we have included the corresponding values for the dust-corrected samples ($LR_{\text{dust}}^{\text{obs}}$), while for simulated DLAs the filtered ($LR_{\text{fil}}^{\text{sim}}$) estimations are also displayed.

X	LR^{obs}	$LR_{\text{dust}}^{\text{obs}}$	$\sigma_{z_{\text{low}}}^{\text{obs}}$	$\sigma_{z_{\text{inter}}}^{\text{obs}}$	LR^{sim}	$LR_{\text{fil}}^{\text{sim}}$	$\sigma_{z_{\text{low}}}^{\text{sim}}$	$\sigma_{z_{\text{inter}}}^{\text{sim}}$
[Fe/H]	-0.17 ± 0.11	-0.31 ± 0.14	0.42	0.68	-0.36 ± 0.05	-0.36 ± 0.04	0.59	0.58
[Zn/H]	-0.28 ± 0.13	-0.28 ± 0.13	0.39	0.65	-0.26 ± 0.03	-0.26 ± 0.03	0.33	0.44
[Si/H]	-0.19 ± 0.24	-0.22 ± 0.24	0.15	0.12	-0.29 ± 0.06	-0.32 ± 0.03	0.45	0.48
[Si/Fe]	-0.02 ± 0.09	0.09 ± 0.08	0.10	0.31	0.05 ± 0.01	0.04 ± 0.01	0.18	0.13

Table 2. Intrinsic Evolution: difference between unweighted means estimated at redshift bins z_{low} and z_{inter} for both observed and simulated DLAs (bootstrap errors given).

[X/Y]	$\Delta\langle[X/Y]^{\text{obs}}\rangle_{\text{u}}$	$\Delta\langle[X/Y]_{\text{dust}}^{\text{obs}}\rangle_{\text{u}}$	$\Delta\langle[X/Y]^{\text{sim}}\rangle_{\text{u}}$	$\Delta\langle[X/Y]_{\text{fil}}^{\text{sim}}\rangle_{\text{u}}$
[Fe/H]	-0.09 ± 0.18	-0.06 ± 0.24	-0.33 ± 0.11	-0.21 ± 0.08
[Zn/H]	-0.05 ± 0.20	-0.05 ± 0.20	-0.23 ± 0.09	-0.03 ± 0.09
[Si/H]	-0.03 ± 0.20	-0.02 ± 0.20	-0.29 ± 0.12	-0.19 ± 0.08
[Si/Fe]	-0.12 ± 0.08	-0.08 ± 0.05	-0.02 ± 0.09	0.02 ± 0.02

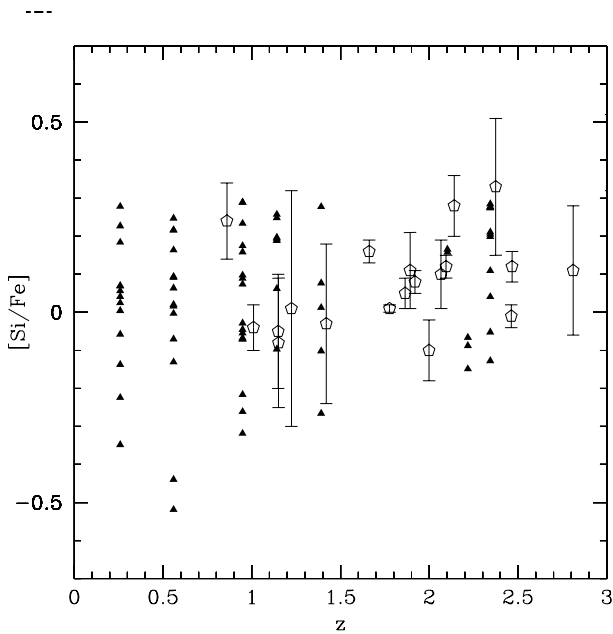


Figure 5. [Si/Fe] versus redshift for the neutral hydrogen in DLAs (*filled triangles*). Dust corrected observational data have been included for comparison (Valdilo 2002, *open pentagons*).

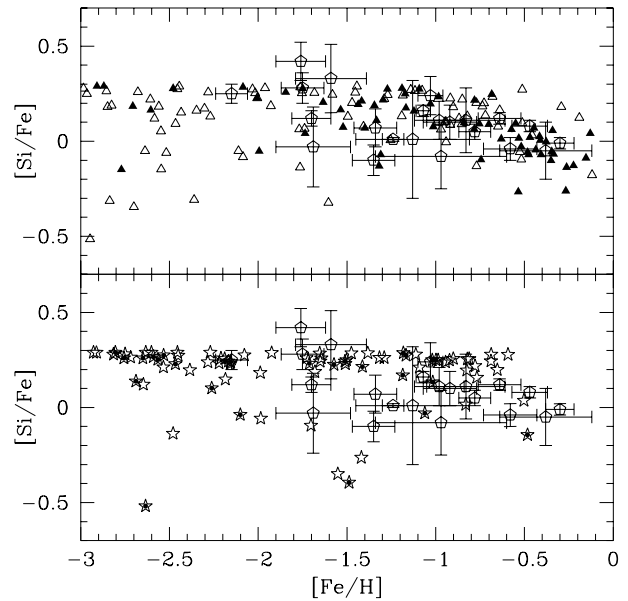
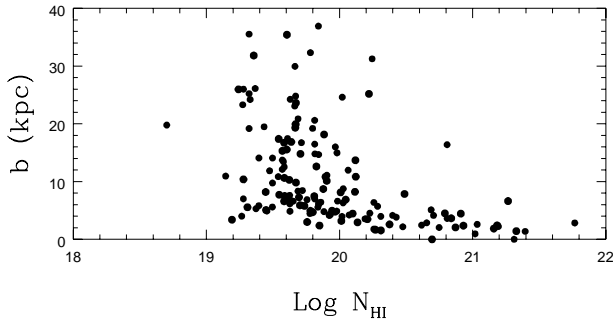
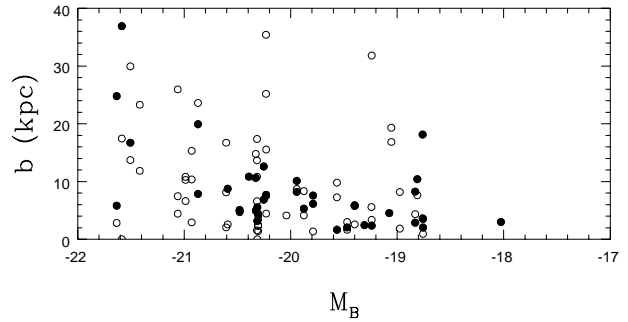


Figure 6. [Si/Fe] versus [Fe/H] for the neutral hydrogen (a) and the stellar populations (b) in DLAs (*filled triangles* and *dotted stars*, respectively) and sub-DLAs (*open triangles* and *stars*, respectively). Dust corrected observational data have been included for comparison (Valdilo 2002, *open pentagons*).

Table 3. Global Evolution: difference between H_I mass weighted means estimated at redshift bins z_{low} and z_{inter} for both observed and simulated DLAs (bootstrap errors given).

[X/Y]	$\Delta\langle[X/Y]^{\text{obs}}\rangle_w$	$\Delta\langle[X/Y]_{\text{dust}}^{\text{obs}}\rangle_w$	$\Delta\langle[X/Y]^{\text{sim}}\rangle_w$	$\Delta\langle[X/Y]_{\text{fil}}^{\text{sim}}\rangle_w$
[Fe/H]	-0.12 ± 0.08	-0.31 ± 0.35	-0.85 ± 0.48	-0.24 ± 0.21
[Zn/H]	-0.30 ± 0.34	-0.30 ± 0.34	-0.51 ± 0.39	-0.14 ± 0.04
[Si/H]	-0.04 ± 0.23	-0.19 ± 0.37	-0.72 ± 0.59	-0.27 ± 0.09
[Si/Fe]	-0.29 ± 0.10	-0.04 ± 0.08	-0.32 ± 0.12	-0.18 ± 0.05

**Figure 7.** Impact parameter versus H_I column density for LOSs drawn through galaxy-like objects in the redshift range $0.26 < z < 2.35$.**Figure 8.** Impact parameter b (kpc) as a function of the blue absolute magnitude M_B for simulated DLAs and sub-DLAs at $z < 1$. We have distinguished between those satisfying the observational constrain $18.8 < \log N(H_I) + [Zn/H] < 21$ (*filled circles*) and those outside this observational window (*open circles*).

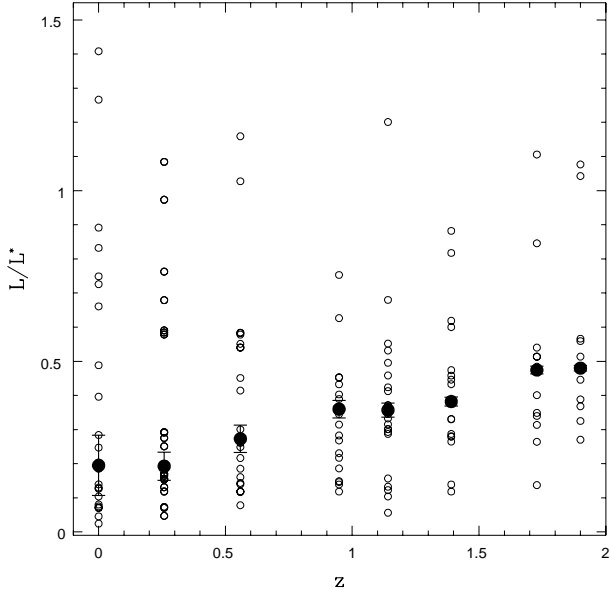


Figure 9. The median blue luminosity of building blocks that host the $N(\text{H}_I)$ absorptions normalized to L_B^* at $z = 0$ as a function of z (*filled circles*). Bootstrap errors are shown. We have also included the individual ratios (*open circles*).

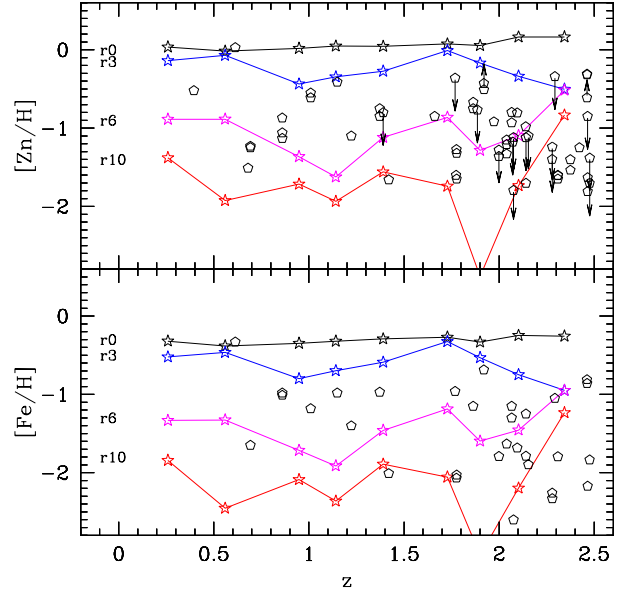


Figure 11. $\langle[\text{Zn}/\text{H}]\rangle$ and $\langle[\text{Fe}/\text{H}]\rangle$ unweighted mean abundances as a function of redshift for stars in GLOs (*empty stars*) further than a certain radius from the centre of the simulated galactic objects. Connected symbols from the top to the bottom represent inner cut-off radius of $r_0 = 0$, $r_3 = 3$, $r_6 = 6$ and $r_{10} = 10$ kpc, respectively. Observational data is represented by *open pentagons*

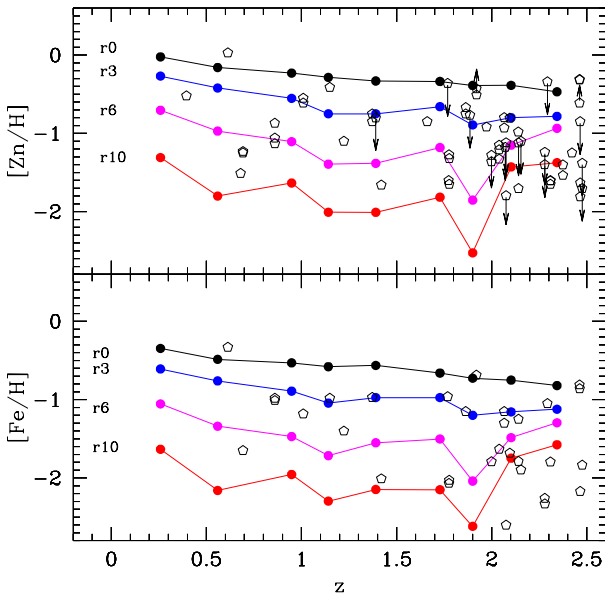


Figure 10. $\langle[\text{Zn}/\text{H}]\rangle$ and $\langle[\text{Fe}/\text{H}]\rangle$ unweighted mean abundances as a function of redshift for gas in GLOs (*filled circles*) further than a certain radius from the centre of the simulated galactic objects. Connected symbols from the top to the bottom represent inner cut-off radius of $r_0 = 0$, $r_3 = 3$, $r_6 = 6$ and $r_{10} = 10$ kpc, respectively. Observational data is represented by *open pentagons* (Vladilo 2002)